Nanoscale

Accepted Manuscript

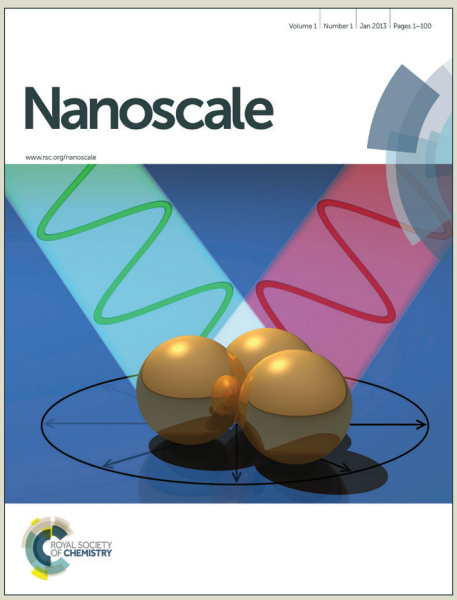

ROYAL SOCIETY OF CHEMISTRY

www.rsc.org/nanoscale

Journal Name

RSCPublishing

ARTICLE

Polyhydroxylated [60]Fullerene Binds Specifically to Functional Recognition Sites on Monomeric and Dimeric Ubiquitin

Cite this: DOI: 10.1039/xoxxoooooox

Received ooth January 2012,
Accepted ooth January 2012

DOI: 10.1039/xoxxoooooox

www.rsc.org/

Serena Zanzoni,[a] Alberto Ceccon,[a] Michael Assfalg,[a] Rajesh K. Singh,[b] David Fushman,[b] and Mariapina D'Onofrio[a]

The use of nanoparticles (NPs) in biomedical applications requires an in-depth understanding of the mechanisms by which NPs interact with biomolecules. NPs associating with proteins may interfere with protein-protein interactions and affect cellular communication pathways, however the impact of NPs on biomolecular recognition remains poorly characterized. In this respect, particularly relevant is the study of NP-induced functional perturbations of proteins implicated in the regulation of key biochemical pathways. Ubiquitin (Ub) is a prototypical protein post-translational modifier playing a central role in numerous essential biological processes. To contribute to an understanding of the interactions between this universally distributed biomacromolecule and NPs, we investigated the adsorption of polyhydroxylated [60]fullerene to monomeric Ub and to a minimal polyubiquitin chain *in vitro* at atomic resolution. Site-resolved chemical shift and intensity perturbations of Ub's NMR signals, together with ^{15}N spin relaxation rate changes, exchange saturation transfer effects, and fluorescence quenching data were consistent with the reversible formation of soluble aggregates incorporating fullerenol clusters. Specific interaction epitopes were identified, coincident with functional recognition sites in monomeric and lysine48-linked dimeric Ub. Fullerenol appeared to target the open state of the dynamic structure of dimeric Ub according to a conformational selection mechanism. Importantly, protein-NP association prevented enzyme-catalyzed synthesis of polyubiquitin chains. Our findings provide experiment-based insight into protein/fullerenol recognition, with implications in functional biomolecular communication, including regulatory protein turnover, and for the opportunity of therapeutic intervention in Ub-dependent cellular pathways.

Introduction

Life is sustained by a finely tuned network of biomolecular interactions. Exposure of living organisms to exogenous agents such as nanoparticles (NPs) may cause interfering associations, sometimes leading to dramatic biological consequences.[1–3] However, the current knowledge on NP interactions with biomolecules remains scarce. In this respect, particularly relevant is the study of NP-induced functional perturbations of proteins implicated in the regulation of key biochemical pathways. Herein we focus on ubiquitin (Ub), a small protein acting as a post-translational modifier upon covalent conjugation to protein substrates and playing a central role in numerous processes including protein degradation, cell signaling, and DNA repair.[4]

Ub modifies target proteins *via* an isopeptide linkage between its carboxyl terminus and a lysine residue of the substrate. Additional covalent bonds between Ub monomers, generally involving one of the seven Ub lysine residues, may lead to polyUb chain formation.[5] Substrate conjugation by monomeric Ub or structurally diverse Ub chains elicits distinct downstream responses which originate from molecular recognition involving specific and distinct Ub surface patches.[6] For example, a hydrophobic surface patch including Leu8, Ile44, and Val70 mediates the interaction of Ub units in Lys48-linked chains with Ub-binding motifs of partner proteins in the Ub/proteasome proteolytic pathway.[7] Notably, ubistatin binding to this hydrophobic patch was shown to interfere with its recognition by Ub chain receptors of the proteasome, offering an opportunity for cancer drug development.[8]

Monomeric Ub has a stable globular fold which has been thoroughly characterized in solution as well as in crystal form. Recent investigations made use of Ub as a test biomolecule to describe NP-protein interactions. Ub was reported to interact specifically with citrate-coated gold NPs[9] and to bind citrate-coated silver NPs.[10] The adsorption of Ub to uncoated silver NPs resulted in the formation of insoluble aggregates incorporating amyloid-like structures.[10] Residues distributed over the entire β-sheet domain displayed the largest NMR spectral perturbations in the presence of silver NPs. A recent

computational study of the interaction between Ub and hydroxylated [60]fullerene identified two specific binding sites on the protein surface, mapping to the region around Tyr59 and to the C-terminus.[11]

In this work we studied the interactions of fullerene NPs with both monomeric and dimeric Ub in order to understand their potential impact of carbon NPs on life-essential processes. Fullerenes and their derivatives have attracted interest in several areas of biology and medicine due to unique physical and chemical properties.[12] Potential biomedical applications include their use as drug carriers, antiviral drugs, enzyme inhibitors, contrast agents, antioxidants, and photosensitizers.[12] The most commonly occurring member of the family, [60]fullerene (C_{60}), consists of sixty carbon atoms arranged in a truncated icosahedron.[13] Pristine C_{60} is essentially insoluble in aqueous media, an unfavourable property for its release in a biological environment. Exohedral functionalization with polar groups has the advantage of increasing water solubility. Hydroxylation of the carbon cage results in molecules known as fullerenols or poly(hydroxy)fullerenes [$C_{60}(OH)_x$], as well as fullerenol salts ([$C_{60}(OH)_xO_y^-$][K,Na^+]$_y$).[14,15]

We describe the interactions between fullerenol and the Ub system, providing atomic-level insight into the structural organization of the formed soluble aggregates. We adopted site-resolved NMR spectroscopy, which was recently introduced for the characterization of nano-bio interfaces,[9,16–18] together with fluorimetry and size-exclusion chromatography. We further applied the recently described dark-state exchange saturation transfer experiment as a unique tool to demonstrate the reversibility of protein-nanoparticle association,[19,20] and used nuclear spin relaxation to derive information about the hydrodynamic properties of the nanoscale conjugates. For the identification of surface patches on di-ubiquitin we adopted segmental isotope labelling.[21] The impact of fullerenol on polyubiquitin chain synthesis was assessed by polyacrylamide gel electrophoresis. We discuss the implications of our findings in the context of Ub-mediated cellular signalling pathways.

Results and discussion

Fullerenol clusters adsorb reversibly to monomeric Ub

We investigated the association of fullerene NPs with Ub by performing heteronuclear correlation NMR experiments. Preparations of Ub in the presence of pristine C_{60}, obtained with the aid of ultrasonication, resulted in unperturbed $^1H,^{15}N$-HSQC (heteronuclear single quantum coherence) protein spectra (not shown), ruling out any significant association with the NPs. In the conditions used, we found no evidence to support the prediction, based on discrete molecular dynamics simulations, that Ub misfolds in the presence of pristine C_{60}.[11] We therefore decided to explore the interaction of Ub with water soluble fullerene derivatives. As a compromise between preserving part of the surface chemistry of pristine C_{60} and increasing solubility we selected a medium-degree hydroxylated derivative[14] (24 OH/O^- groups, hereafter referred to as fullerenol, Figure 1a). These particles are reported to occur in solution mostly as soluble clusters due to extended hydrophobic and π-π interactions.[22] Consistently, by dynamic light scattering we found a bi-modal particle-size distribution with a major peak centered at 6 nm (Figure S1 in the Electronic Supplementary Information (ESI)).

The addition of fullerenol to Ub samples resulted in clear solutions with no precipitates. In fluorimetric experiments, the fluorescence emission intensity of excited Tyr59 decreased progressively upon addition of fullerenol (Figure 1b). The normalized intensity change displayed a nonlinear trend as a function of total fullerenol concentration (Figure 1c), attributable to a static quenching effect due to formation of a nonfluorescent ground-state complex.[23] The protein-NP interaction was further confirmed by size exclusion chromatography (Figure S2).

To explore the hydrodynamic properties of the observable species in solution we performed ^{15}N longitudinal spin relaxation rate measurements, ^{15}N R_1, on Ub upon subsequent additions of fullerenol. ^{15}N R_1 data were used to derive the apparent rotational correlation time constant, τ_c, at each titration step (see Experimental Section for details). The τ_c value of Ub increased progressively after the second addition until fullerenol was in twofold molar excess, and at [fullerenol]/[Ub] = 4 it reached the value of 9.5 ns, which is a factor of 2.2 larger than the τ_c of free Ub (Figure 1d). These results indicate that the observed species in solution in advanced titration steps departed from a simple binary complex formed by one Ub and one fullerenol particle (expected to exhibit a τ_c below 4.5 ns), instead the data are consistent with interactions involving fullerenol clusters. The rotational correlation time observed at saturation could originate from different protein/NP stoichiometries. By approximating all molecules and assemblies as spherical bodies, and applying the Stokes-Einstein-Debye law, we estimated that an assembly formed by one Ub molecule and 40 fullerenol particles would display a τ_c value of about 9.4 ns. A similar τ_c value could be expected for a complex comprising two Ub molecules and 10 fullerenol particles, a more likely scenario based on our titration data.

The reversibility of the protein-NP interaction was inferred from the hyperbolic-like trend observed for the global ^{15}N R_1 values plotted against the fullerenol concentration (Figure S3). Additional compelling evidence was obtained from dark-state exchange saturation transfer experiments (DEST).[19] In the DEST experiment, the ^{15}N magnetization of an observable species undergoing reversible association with a slowly tumbling aggregate is transferred by chemical exchange to the NMR-invisible state, partly saturated, and transferred back upon dissociation. The observation of a slightly broader saturation profile for the 1D H_N envelope of the Ub spectrum in the presence of fullerenol ([fullerenol]/[Ub] = 0.75, Figure 1e) supported an equilibrium exchange process between free and bound Ub forms occurring during the saturation time (0.9 s).[20,24]

Identification of the fullerenol binding epitope on monomeric Ub

To obtain atomic-level information about the interaction between fullerenol and Ub, NMR $^1H,^{15}N$-HSQC spectra were acquired for Ub alone and after stepwise addition of fullerenol (Figure 2a). The ^1H_N and ^{15}N resonance frequencies (chemical shifts) are sensitive to chemical environment and therefore can serve as exquisite reporters of interactions. Several peak position changes were observed during the titration (Figure 2). Analysis of chemical shift perturbations (CSPs) resulted in the identification of two mostly perturbed regions centered around residues Ile44 and Val70, together forming a contiguous area on the Ub surface defined by residues in strands β3-β5 (Figure 1f, 4a,4b). Concomitant with CSP, a decrease in peak intensities was also observed (Figure 2c) and many signals

became undetectable at [fullerenol]/[Ub] > 1.5. Intensity perturbations varied along the protein sequence and matched closely the CSP profile, although with a stronger effect around Leu8.

The fullerenol contact surface on Ub consists of the hydrophobic patch centered around Leu8, Ile44 and Val70, extending to the C-terminus and part of strands β3 and β5 (Figure 4a,b). The borders of this area include residues Phe45 and Leu71, belonging to the two non-contiguous fullerenol binding sites predicted by computational studies.[11] The side chains present in this region likely establish hydrophobic interactions with the fullerenol rings, supported by salt bridges or cation-π interactions involving the guanidino groups of Arg42 and Arg72 and the amino groups of Lys6 and Lys48, and additional polar contacts with the hydroxyl groups of fullerenol. His68 and Phe45 could provide additional stabilizing energy through π-π interactions.

The side chains of amino acid residues forming the fullerenol interaction epitope cover a molecular surface area of ~12 nm^2, corresponding to the projection surface of a layer of 10-12 closely packed fullerenol particles. The soft, possibly dynamic, nature of fullerenol clusters does not allow to determine a precise stoichiometry on the basis of simple geometric considerations or to distinguish unambiguously whether one or two Ub molecules are involved in formation of the assembly. Furthermore, we cannot rule out that Ub-Ub contacts also contribute to the observed NMR perturbation patterns. Nonetheless, it is clear that fullerenol clusters adsorb to Ub differently than other hard NPs. The observed interaction epitope differs in surface area and position from that reported for the binding to citrate-coated gold nanoparticles (epitope formed by residues Gln2, Ile3, Leu15, Val17 and Glu18).[9] The binding to uncoated silver NPs was shown to perturb a more extended area than that interacting with fullerenol,[10] more closely resembling the surface involved in non-covalent dimer formation at high Ub concentrations.[25] Thus, distinct Ub surface patches are selected by different NPs, depending on particle surface chemistry and size.

Physiological relevance of fullerenol binding to Ub

Evidence has been accumulated that water soluble fullerene derivatives can be taken up by cells[26–29] and that the efficiency of fullerenol internalization can become significant in the presence of polycationic transfection agents.[29] Ub is universally distributed among eukaryotic cells and thus it is likely to eventually associate with internalized NPs. The changes in ^{15}N R_1 value as a function of fullerenol/Ub molar ratio (Figure S3) were used to evaluate the binding affinity. In a first analysis the stoichiometry was introduced as an adjustable parameter and was found to be close to 1:1. This apparent contradiction with the proposed higher order stoichiometry (e.g. two Ub and ten fullerenol molecules) can be explained by the fact that in the present system affinity is dictated by the concentration of the single fullerenol molecule, presumably as a consequence of a highly dynamic equilibrium between monomeric and aggregated states of fullerenol. This finding is in agreement with the expectation that a model in which fullerenol clusters of constant defined composition bind to the protein with fixed stoichiometry is not realistic, given the dynamic nature of the clusters. Therefore, assuming a simple two-state association equilibrium between Ub and fullerenol, we estimated an apparent dissociation constant, K_d = 200 ± 88 μM. Although crudely estimated, the strength of this interaction is comparable with that of protein-protein complexes formed by Ub and partner proteins. As an example, the binding of Ub with isolated ubiquitin associated domains (UBA) was found to display an affinity in the range 20-500 μM.[30] Thus, fullerenol particles may effectively interfere with protein-mediated functional communication, eliciting cytotoxic effects.

We examined whether the interaction of fullerenol could affect the formation of polyUb chains. The latter process can be achieved *in vitro* after mixing Ub with small amounts of Ub-activating enzyme E1 and the Ub-conjugating enzyme E2.[31] We monitored the reaction products obtained in the absence and presence of fullerenol using sodium dodecyl sulfate (SDS)-polyacrylamide gel electrophoresis (PAGE) and found that fullerenol almost completely abolished formation of Ub_2 and longer chains (Figure 5). This result can be explained by the fact that the fullerenol contact surface on Ub includes the regions around both residues involved in isopeptide bond formation, Lys48 and Gly76 (Figure 4a,b), thereby preventing molecular recognition. Because the use of sub-stoichiometric fullerenol concentrations did not impair polyUb production, we conclude that functional recognition during the reaction is abolished by fullerenol binding to Ub.

Fullerenol particles bind specifically to dimeric Ub

We investigated the ubiquitin dimer, Ub_2, formed by two Ub monomers linked covalently through an isopeptide bond connecting the carboxy-terminal Gly76 of the so-called distal Ub and the ε-amino group of Lys48 in the proximal Ub. The fluorescence quenching effect produced by fullerenol on Ub_2 was larger than that observed with monomeric Ub at the same concentration of fluorophore (Figure 1c), suggesting a cooperative binding with the dimeric form or the interaction with a distinct surface patch. The binding affinity was reduced (reduced quenching effect) in higher ionic strength condition (Figure 1c), indicating that electrostatic interactions contributed to the binding energy. Formation of soluble aggregates containing Ub_2 was confirmed by the analysis of R_1 values measured in the presence of increasing fullerenol concentration. The corresponding τ_c values show a very similar trend to that observed for Ub (Figure 1d) and reach the value of >12 ns in the presence of a fourfold excess of fullerenol.

To resolve the NMR signals of the two Ub units in Ub_2, which are almost indistinguishable due to their structural identity, we adopted an established strategy of segmental isotope labelling.[21] Two different protein samples, in which either the proximal [Ub_2(^{15}N-P)] or the distal [Ub_2(^{15}N-D)] unit was enriched in ^{15}N, were mixed with increasing amounts of fullerenol, and ^{1}H,^{15}N-HSQC spectra were recorded (Figure 3a,b). Peak position changes were observed for both samples throughout the titrations (Figure 3c,d), indicating that the chemical environments of both units were perturbed by the presence of fullerenol. The strongest effects were observed in discrete regions of the polypeptide chain, particularly around positions 48 and 70. The CSP patterns appear similar for the two Ub units, while the CSP magnitudes are somewhat stronger for the distal than for the proximal Ub at equivalent amounts of NPs, suggesting preferential binding to the former. A differential behavior is particularly evident from analysis of intensity perturbations. As in the case of Ub, NMR peaks exhibited an intensity decrease upon addition of fullerenol, the extent of this effect being region-specific and analogous to the CSP pattern (Figure 3e-h). Therefore signal intensities not only reported on a global population shift towards larger

supramolecular species but also on specific association equilibria occurring in an intermediate exchange regime.

Potential impact of fullerenol on the ubiquitin/proteasome degradation pathway

The fullerenol binding surface on both the distal and proximal units of Ub_2 maps to an analogous patch to that described for Ub (Figure 4c,d). Importantly, however, there is a preference for binding to the distal Ub, likely reflecting the asymmetric modification of the chemical environment after conjugation of the two monomers. As in the case of Ub, it cannot be ruled out that Ub_2-Ub_2 contacts may also contribute to the observed NMR perturbations. Analysis of the ^{15}N R_1 binding isotherm (Figure S3) resulted in an apparent $K_d = 75 \pm 40$ μM, indicating a stronger affinity of fullerenol for Ub_2 compared to Ub. A similar trend was observed for the binding of Ub and Lys48-linked Ub_2 to both UIM-2 of the proteasomal subunit S5a and the UBA2 domain of the DNA repair protein HHR23A.[32,33] In the latter case, the stronger affinity of UBA2 for Lys48-linked Ub_2 was attributed to the formation of a Ub-UBA2-Ub 'sandwich-like' structural arrangement, specific of polyUb chains bearing a Lys48 linkage.[33] A similar conformation could be involved in cooperative binding to fullerenol clusters.

Ub_2 and higher order polymers are inherently dynamic and are best described as ensembles of different conformations in equilibrium.[21,34–37] Lys48-linked Ub_2 was shown to adopt a 'closed' structure, where the Leu8-Ile44-Val70 hydrophobic patches on each domain contact each other, and an 'open' conformation in which the two monomeric units are farther apart. Because we did not observe additional perturbations outside the interdomain surface, the hydrophobic patches also serve as fullerenol binding sites. It seems likely that fullerenol may interact with Ub_2 according to the same conformational selection mechanism proposed for the interaction with Ub interacting proteins,[37,38] targeting the Ub_2 epitope in the open state and therefore competing effectively with functional molecular recognition.

Cellular proteins conjugated to Lys48-linked polyUb chains are targeted for proteasomal degradation, the principal regulatory mechanism of protein turnover.[39] Recognition of poly-Ub tagged substrates by the proteasome appears to be mediated by shuttle proteins bearing Ub-binding domains, such as UBA in Rad23 proteins.[40] Failure to form controlled protein assemblies along the degradation pathway can result in impaired function of the proteasomal machinery and accumulation of polyubiquitinated substrates. In this regard, it was previously shown that fullerenol treatment causes accumulation of ubiquitinated proteins in cultured vascular endothelial cells,[28] confirming the impact of this NP on protein degradation by the Ub/proteasome system. The latter has been suggested as an attractive target for cancer drug development. In analogy with Ub-chain-directed drugs, ubistatins, which were shown to disrupt recognition by Ub-chain receptors,[8] fullerenol NPs may provide an alternative scaffold for the development of inhibitors of proteasome-dependent degradation, leading to cell-cycle arrest, ultimately offering a novel opportunity for the treatment of malignant tumours.

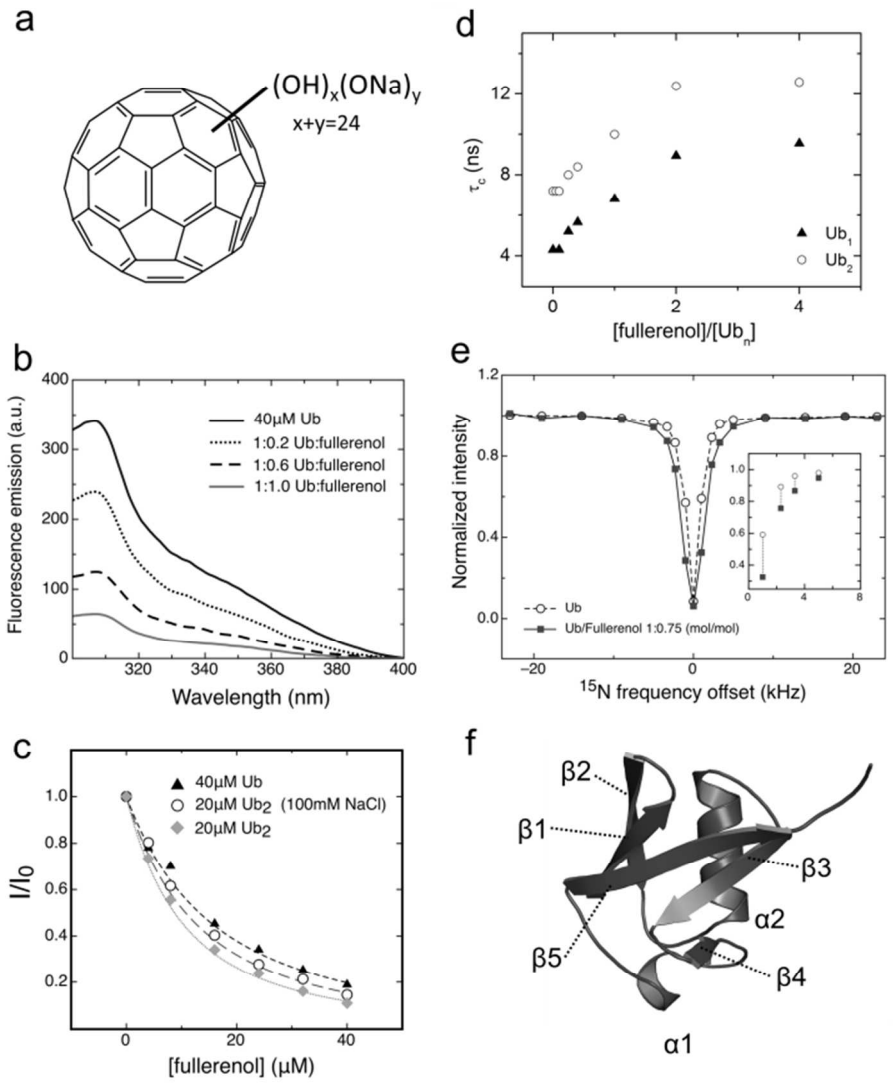

Figure 1. Evidence of fullerenol binding to Ub and Ub_2. a) Chemical structure of the fullerenol particle used in this study. b) Fluorescence emission spectra of Ub (Tyr59, excitation at 280 nm) in the presence of fullerenol. c) Normalized maximum emission fluorescence measured on Ub at increasing fullerenol concentration (lines serve to guide the eye). d) Rotational correlation time for Ub and Ub_2 in the presence of fullerenol, determined from ^{15}N spin relaxation measurements. e) Saturation profile of the 1D H_N envelope of Ub by transfer of ^{15}N saturation from the NP-bound state. The inset highlights the intensity differences measured for Ub alone and in the presence of NPs. Errors in intensities were estimated from spectral noise and are about the size of the symbols. f) Cartoon representation of Ub with secondary structure elements indicated.

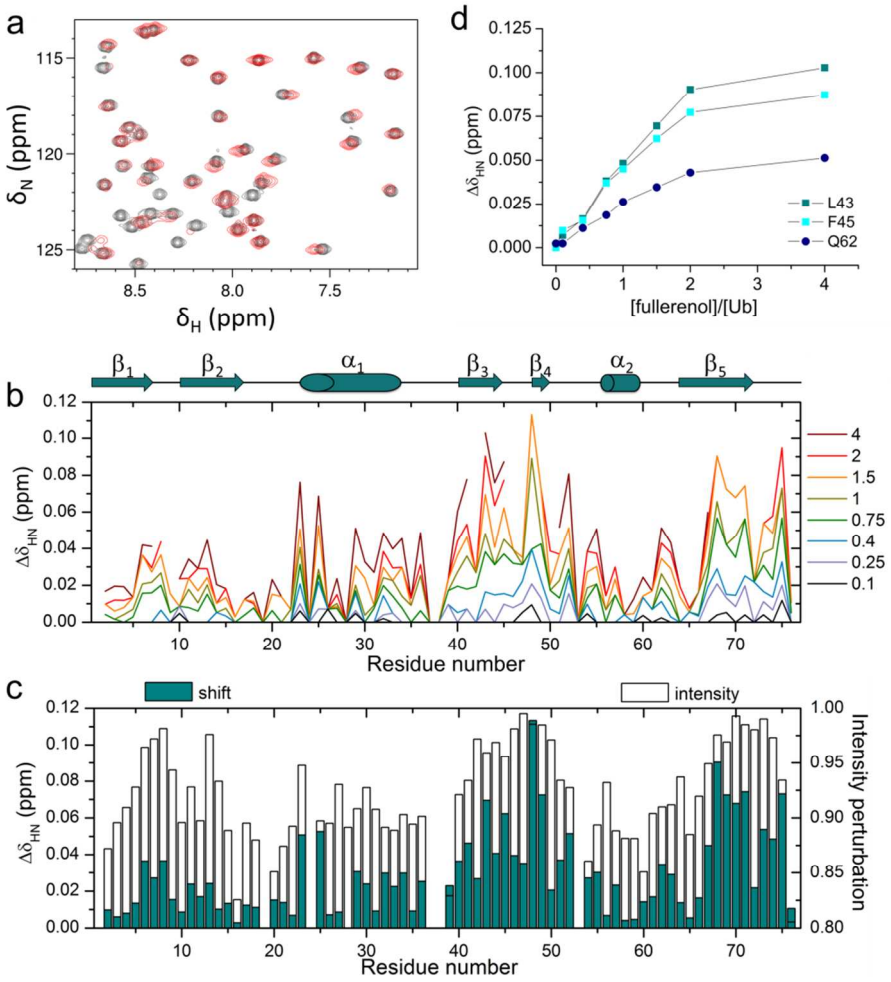

Figure 2. NMR signal perturbations of Ub in the presence of fullerenol. a) Overlaid regions of ^{1}H,^{15}N-HSQC NMR spectra collected on ^{15}N-Ub in the absence (dark grey) and presence (red) of fullerenol at [fullerenol]/[Ub] = 1.5. b) CSPs measured at the [fullerenol]/[Ub] molar ratios reported in the legend. Secondary structure elements are reported on top of the panel. c) CSPs and intensity perturbations measured at [fullerenol]/[Ub] = 1.5. Intensity perturbation was computed as: $(I_0-I_i)/I_0$, where I_i is the signal intensity at titration step i, and I_0 is the signal intensity of free Ub. d) Representative CSP-based binding isotherms.

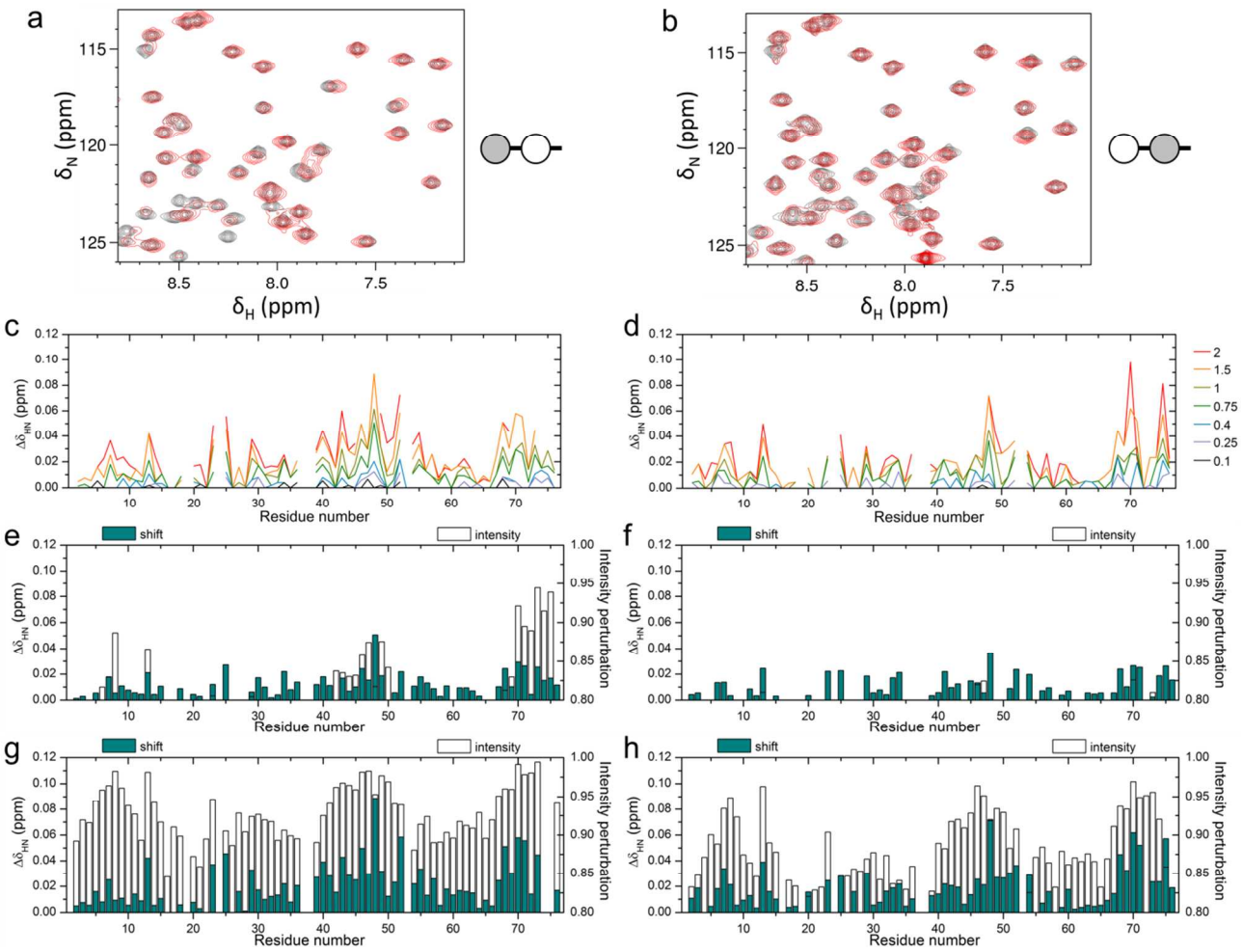

Figure 3. NMR signal perturbations of Ub_2 in the presence of fullerenol. a, b) Overlaid regions of $^{1}H,^{15}N$-HSQC NMR spectra collected in the absence (dark grey) and presence (red) of fullerenol at [fullerenol]/[Ub_2] = 1.5. In the schematic representation of Ub_2 on the right of each spectrum, the ^{15}N-labelled Ub unit is coloured in grey, the unlabelled unit is displayed in white. c, d) CSPs measured at the [fullerenol]/[Ub_2] values indicated in the legend. e, f) CSPs and intensity perturbations measured at [fullerenol]/[Ub_2] = 0.75. g,h) CSPs and intensity perturbations measured at [fullerenol]/[Ub_2] = 1.5. Panels a, c, e, g display data measured on $Ub_2(^{15}N\text{-}D)$ while the data in panels b, d, f, h correspond to $Ub_2(^{15}N\text{-}P)$.

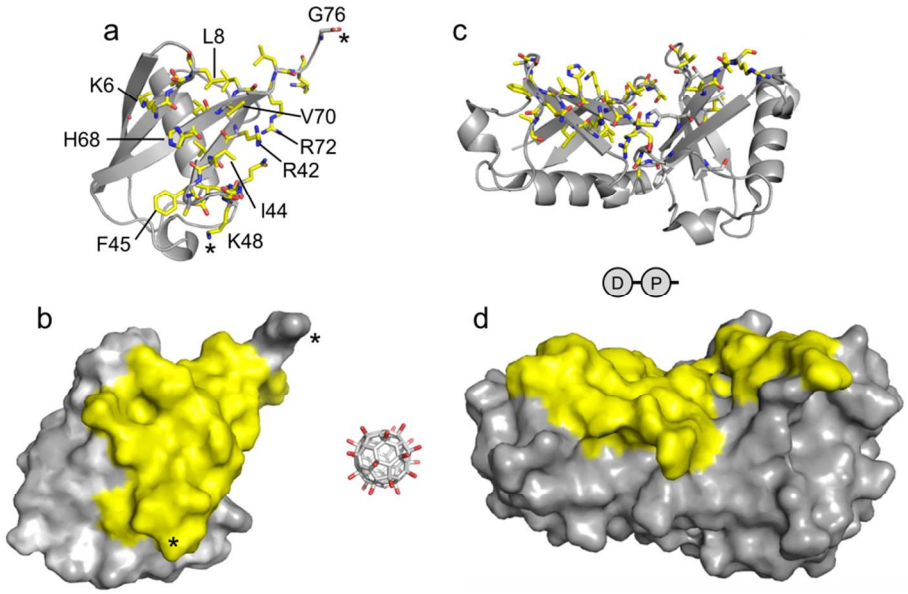

Figure 4. Mapping of the fullerenol binding surface on ubiquitin. a) Mapping of Ub residues (yellow sticks) displaying greater-than-average intensity perturbations after addition of fullerenol ([fullerenol]/[Ub] = 1.5); key interface residues are indicated; asterisks indicate the sites of covalent modification involved in formation of Lys48-linked chains; the shown structure is 1UBQ. b) Ub molecular surface with the fullerenol-binding epitope painted yellow. c) Mapping of Ub_2 residues (yellow sticks) displaying greater-than-average intensity perturbations after addition of fullerenol ([fullerenol]/[Ub_2] = 1.5); yellow colored residues in the proximal Ub correspond to an intensity attenuation > 0.95, the residues that exhibited an intensity attenuation between 0.93 and 0.95 are shown in gray sticks; the distal (carrying free Lys48) and proximal (carrying free C-terminus) units are schematically depicted in the bottom; the figure corresponds to the 'open' solution structure 2PE9. d) Molecular surface of Ub_2 with the fullerenol-binding epitope painted yellow. A fullerenol molecule is shown between panels b and d in scale with all proteins displayed in the figure.

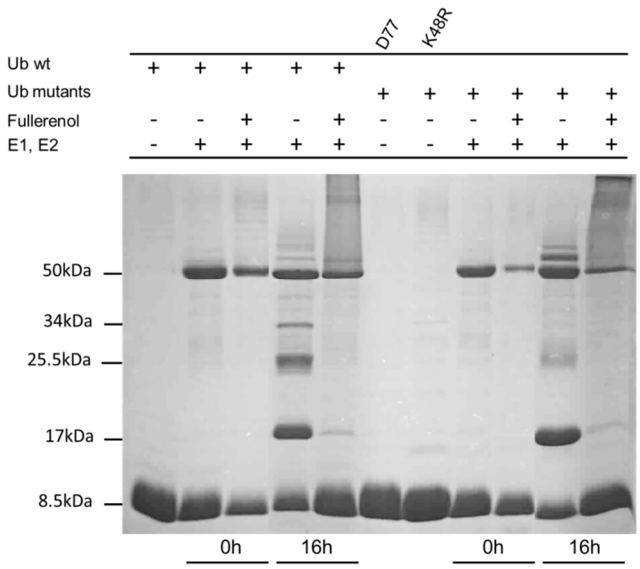

Figure 5. PolyUb chain formation monitored by SDS-PAGE. Ub and its mutants Ub(K48R) and Ub(D77) have a molecular weight of ~8.5 kDa. Ub_2, Ub_3, and Ub_4 have molecular weights of 17, 25.5, and 34 kDa, respectively. GST-E2 has a molecular weight of about 50 kDa. Addition of fullerenol at the same molar concentration as Ub abolished polyUb chain formation. Results for Ub(K48R) and Ub(D77) are shown as these mutants were used for Ub_2 production in all experiments described in this work. These mutations prevent formation of chains longer than the dimer.

Conclusions

In summary, we performed an atomic-level characterization of a prototypical monomeric and multidomain protein modifier in the presence of a water soluble fullerene. The combination of a variety of NMR techniques proved a powerful tool to describe in detail the formation of dynamic assemblies between biomolecules and nanomaterials. Our findings support the view that fullerenol NPs may affect fundamental interaction patterns, with possible nanotoxic consequences on cell homeostasis. The specific inhibition of critical Ub/proteasome interactions through competitive binding of NPs to polyUb chains represents a novel potential opportunity for pharmacological intervention against cancer development.

Experimental

Chemicals

Fullerene (purity > 99.9 %) and fullerenol (purity > 95 %) were purchased from Materials and Electrochemical Research Corporation (Tucson, AZ) and examined by DLS. All other chemicals used in the work were supplied from Sigma.

Protein expression and purification and polyUb chain synthesis

Unlabeled and uniformly ^{15}N-labeled recombinant Ub and protein mutants, Ub (K48R) and Ub (D77), were expressed and purified as described.[41] Segmentally isotope-labeled Ub_2 chains were synthesized as described in Varadan et al.[21] using enzymes E1 and E2 in overnight reactions at 37 °C added with ATP, TCEP, and an ATP reconstituting cocktail. Products of polyUb synthesis were identified by SDS-PAGE. Proximal ^{15}N-labeled Ub_2 (here referred to as Ub_2-P) was synthesized by using ^{15}N Ub (D77) and unlabeled Ub (K48R); distal ^{15}N-labeled Ub_2 (Ub_2-D) was synthesized using ^{15}N Ub (K48R) and unlabeled Ub (D77). Ub_2 was separated from unreacted Ub monomers at the end of the reaction by cation-exchange chromatography and the Ub_2 concentration was determined from UV absorbance. For all protein samples ^{1}H-1D and ^{1}H,^{15}N-HSQC spectra were acquired to confirm sample purity and structural integrity.

Size exclusion chromatography

Ub samples and Ub adducts with NPs were analyzed by size-exclusion gel-filtration chromatography through a Superdex G75 xk 16/70 column (GE Healthcare), equilibrated with 10 mM potassium phosphate (K_2HPO_4/KH_2PO_4) buffer pH 6.8, 0.02% NaN_3. Sample concentration was the same used for NMR experiments. 2 ml fractions were collected and size-separated by 15% SDS-PAGE stained with Coomassie blue.

NMR experiments

All NMR spectra were recorded on a 600 MHz Bruker Avance III spectrometer equipped with a triple resonance TCI cryogenic probe. The measurement temperature was 25 °C for all experiments. NMR samples were prepared in a 10 mM potassium phosphate buffer, pH 6.8, 5% D_2O, 0.02% NaN_3. The protein concentration was 0.4-0.8 mM.

Typical ^{1}H,^{15}N-HSQC experiments were recorded with a data matrix consisting of 2048 (F2, ^{1}H) × 128 (F1, ^{15}N) complex points. The number of scans was 16 and the relaxation delay 2 s. Spectral windows of 9615 (F2) and 2067 (F1) Hz were used. Chemical shift perturbations were calculated as $CSP = [(\Delta\delta_H)^2+(\Delta\delta_N/5)^2]^{0.5}$, where $\Delta\delta_H$ and $\Delta\delta_N$ are chemical shift changes detected for ^{1}H and ^{15}N signals, respectively.

Protein amide ^{15}N-T_1 experiments were performed in an interleaved fashion, recording only the first increment for each relaxation delay. Optimal water signal suppression was obtained with a flip-back pulse. The recycle delay was 3 s and T_1 relaxation delays were 0.01, 0.18 (duplicate), 0.36, 0.54, 0.72, 0.90 (duplicate) s. Relaxation times T_1 were determined by fitting the integral area of the amide region of each experiment to a single exponential decay using the computer program RELAXFIT.[42] R_1 (= T_1^{-1}) binding isotherms (Figure S3) were analyzed assuming the fast-exchange condition: $R_{1obs} = R_{1f} \times (1- f_b) + R_{1b} \times f_b$, where the observed relaxation rate R_1 is a population weighted average of the corresponding values for the free and bound states, and f_b is the bound protein fraction.[42] The dissociation constant, K_d, was obtained by least-squares fitting of experimental data according to a 1:1 Ub:NP binding model. Relaxation time constants T_1 were finally converted into rotational correlation time constants, τ_c, based on known equations,[43] under the approximation of isotropic motion, assuming a squared order parameter $S^2 = 0.85$ and a ^{15}N chemical shift anisotropy of -160 ppm. Predictions of τ_c values based on given volumes were calculated from the Stokes-Einstein-Debye law: $\tau_c = \eta V/(kT)$ where η is the shear viscosity of the solution, V is the particle volume, k is the Boltzmann constant, and T is temperature. The isotropic radii of Ub and of a single fullerenol particle were taken as 1.57 and 0.5 nm, respectively.

^{15}N-DEST experiments were conducted at 25 °C using the pulse sequence available from Dr. Clore's laboratory (http://spin.niddk.nih.gov/clore/), modified to obtain an interleaved pseudo-3D version for direct processing with spectrometer acquisition software (Bruker Topspin 3.2).[20] 1D ^{15}N-DEST experiments were recorded by simply omitting chemical shift evolution in the ^{15}N frequency dimension. ^{15}N continuous wave saturation (350 Hz) was applied for 0.9 s at 17 offset frequencies distributed symmetrically around 0 Hz (-23.0, -19.0, -14.0, -9.0, -5.0, -3.3, -2.3, -1.0, 0.0, 1.0, 2.3, 3.3, 5.0, 9.0, 14.0, 19.0, 23.0 kHz). Forty-eight transients were recorded with an interscan delay of 1.3 s. A 2.1 ms IBURP2 pulse was applied at 8.24 ppm to achieve amide proton decoupling. Water flip-back pulses were used for optimal water suppression. Serial FIDs with no time evolution in ^{15}N were extracted, processed, and integrated (6-10 ppm).

All data were processed and analyzed using TOPSPIN 3.2 (Bruker, Karlsruhe, Germany) and in-house programs written in Matlab (The Mathworks).

Fluorescence spectroscopy

Fluorescence measurements were performed on a FP-8200 spectrophotometer (JASCO, USA) in 10 mM potassium phosphate buffer, pH 6.8, 0.02% NaN_3. The effect of ionic strength on the binding affinity was investigated by adding 100 mM NaCl to the buffer solution. Ubiquitin's Tyr^{59} emission spectra in the presence of fullerenol were recorded between 300 nm and 400 nm with excitation at 280 nm, using 2.5 and 5 nm bandwidths in the excitation and emission pathways, respectively. The concentration of Ub monomer was maintained at 40 μM (protein dilution within 10% v/v) during all the fluorimetric measurements. The experimental run was performed in triplicate, and the results for each titration point are reported as the average of the measurements.

Dynamic light scattering

To investigate the size and zeta-potential of the fullerenol nanoparticles, 100 μM of fullerenol solution was prepared in 10 mM potassium buffered solution, pH 6.8, or in pure water. The measurements were performed at 25 °C using a Zetasizer Nano ZS (Malvern Instruments, Malvern, UK) operating at λ = 633 nm and equipped with a back scattering detector (173°). Samples were allowed to equilibrate in the instrument holder for at least 10 min. before starting measurements. For size analysis, measurements were performed in triplicate. Correlation curves were converted into size distribution plots (Figure S1A,B) using the non-negative least-squares analysis method. The major peak was found to be centered at 5.9 ± 0.19 nm (intensity distribution). Electrophoretic light scattering experiments were performed as seven replicate measurements. The voltage was automatically set to 148 V. The ζ-potential was derived from the electrophoretic mobility by means of the Henry equation. The ζ-potential distribution (Figure S1C) displayed a single peak at -59.4 ± 1.43 mV in water (-49.9 ± 2.96 mV in buffer).

Acknowledgements

This work was supported by Cariverona Foundation (Nanomedicine Initiative Project), by NIH grant GM065334 (to DF), and by the 2012 Cooperint Internationalization Program of the University of Verona (to MD).

Notes and references

[a] Department of Biotechnology, University of Verona, 37134 Verona (Italy), E-mail: mariapina.donofrio@univr.it
[b] Department of Chemistry and Biochemistry, University of Maryland, College Park, MD 20742-3360 (USA)

† Electronic Supplementary Information (ESI) available: Experimental details. Figure S1: Characterization of fullerenol by dynamic light scattering. Figure S2: Size-exclusion chromatography. Figure S3: ^{15}N R_1 spin relaxation rates of Ub and Ub_2 upon subsequent additions of fullerenol. See DOI: 10.1039/b000000x/

1 S. Linse, C. Cabaleiro-Lago, W.-F. Xue, I. Lynch, S. Lindman, E. Thulin, S. E. Radford and K. A. Dawson, *Proc. Natl. Acad. Sci. U. S. A.*, 2007, **104**, 8691–8696.
2 A. Nel, T. Xia, L. Mädler and N. Li, *Science*, 2006, **311**, 622–627.
3 S. R. Saptarshi, A. Duschl and A. L. Lopata, *J. Nanobiotechnology*, 2013, **11**, 26.
4 R. C. Aguilar and B. Wendland, *Curr. Opin. Cell Biol.*, 2003, **15**, 184–190.
5 C. M. Pickart and D. Fushman, *Curr. Opin. Chem. Biol.*, 2004, **8**, 610–616.
6 D. Komander and M. Rape, *Annu. Rev. Biochem.*, 2012, **81**, 203–229.
7 I. Dikic, S. Wakatsuki and K. J. Walters, *Nat. Rev. Mol. Cell Biol.*, 2009, **10**, 659–671.
8 R. Verma, N. R. Peters, M. D'Onofrio, G. P. Tochtrop, K. M. Sakamoto, R. Varadan, M. Zhang, P. Coffino, D. Fushman, R. J. Deshaies and R. W. King, *Science*, 2004, **306**, 117–120.
9 L. Calzolai, F. Franchini, D. Gilliland and F. Rossi, *Nano Lett.*, 2010, **10**, 3101–3105.
10 V. Mangini, M. Dell'Aglio, A. D. Stradis, A. D. Giacomo, O. D. Pascale, G. Natile and F. Arnesano, *Chem. - Eur. J.*, 2014, **20**, 10745–10751.
11 S. Radic, P. Nedumpully-Govindan, R. Chen, E. Salonen, J. M. Brown, P. C. Ke and F. Ding, *Nanoscale*, 2014.
12 S. Bosi, T. Da Ros, G. Spalluto and M. Prato, *Eur. J. Med. Chem.*, 2003, **38**, 913–923.
13 H. W. Kroto, J. R. Heath, S. C. O'Brien, R. F. Curl and R. E. Smalley, *Nature*, 1985, **318**, 162–163.
14 J. Li, A. Takeuchi, M. Ozawa, X. Li, K. Saigo and K. Kitazawa, *J. Chem. Soc. Chem. Commun.*, 1993, 1784.
15 J.-M. Zhang, W. Yang, P. He and S.-Z. Zhu, *Chin. J. Chem.*, 2010, **22**, 1008–1011.
16 M. Calvaresi, F. Arnesano, S. Bonacchi, A. Bottoni, V. Calò, S. Conte, G. Falini, S. Fermani, M. Losacco, M. Montalti, G. Natile, L. Prodi, F. Sparla and F. Zerbetto, *ACS Nano*, 2014, **8**, 1871–1877.
17 S. Shrivastava, S. A. McCallum, J. H. Nuffer, X. Qian, R. W. Siegel and J. S. Dordick, *Langmuir ACS J. Surf. Colloids*, 2013, **29**, 10841–10849.
18 A. Wang, T. Vo, V. Le and N. C. Fitzkee, *J. Phys. Chem. B*, 2014, **118**, 14148–14156.
19 N. L. Fawzi, J. Ying, R. Ghirlando, D. A. Torchia and G. M. Clore, *Nature*, 2011, **480**, 268–272.
20 A. Ceccon, M. Lelli, M. D'Onofrio, H. Molinari and M. Assfalg, *J. Am. Chem. Soc.*, 2014, **136**, 13158–13161.
21 R. Varadan, O. Walker, C. Pickart and D. Fushman, *J. Mol. Biol.*, 2002, **324**, 637–647.
22 H. Mohan, D. K. Palit, J. P. Mittal, L. Y. Chiang, K.-D. Asmus and D. M. Guldi, *J. Chem. Soc. Faraday Trans.*, 1998, **94**, 359–363.
23 J. R. Lakowicz, *Principles of fluorescence spectroscopy*, Springer, New York, 3rd ed., 2006.
24 N. L. Fawzi, J. Ying, D. A. Torchia and G. M. Clore, *Nat. Protoc.*, 2012, **7**, 1523–1533.
25 Z. Liu, W.-P. Zhang, Q. Xing, X. Ren, M. Liu and C. Tang, *Angew. Chem. Int. Ed.*, 2012, **51**, 469–472.
26 T. Xia, M. Kovochich, J. Brant, M. Hotze, J. Sempf, T. Oberley, C. Sioutas, J. I. Yeh, M. R. Wiesner and A. E. Nel, *Nano Lett.*, 2006, **6**, 1794–1807.
27 S. Foley, C. Crowley, M. Smaihi, C. Bonfils, B. F. Erlanger, P. Seta and C. Larroque, *Biochem. Biophys. Res. Commun.*, 2002, **294**, 116–119.
28 H. Yamawaki, *AJP Cell Physiol.*, 2006, **290**, C1495–C1502.
29 S. A. Anderson, K. K. Lee and J. A. Frank, *Invest. Radiol.*, 2006, **41**, 332–338.
30 S. Raasi, R. Varadan, D. Fushman and C. M. Pickart, *Nat. Struct. Mol. Biol.*, 2005, **12**, 708–714.
31 C. M. Pickart and S. Raasi, *Methods Enzymol.*, 2005, **399**, 21–36.

32 A. Haririnia, M. D'Onofrio and D. Fushman, *J. Mol. Biol.*, 2007, **368**, 753–766.
33 R. Varadan, M. Assfalg, S. Raasi, C. Pickart and D. Fushman, *Mol. Cell*, 2005, **18**, 687–698.
34 Y. Ye, G. Blaser, M. H. Horrocks, M. J. Ruedas-Rama, S. Ibrahim, A. A. Zhukov, A. Orte, D. Klenerman, S. E. Jackson and D. Komander, *Nature*, 2012, **492**, 266–270.
35 Y. Ryabov and D. Fushman, *Proteins*, 2006, **63**, 787–796.
36 Y. E. Ryabov and D. Fushman, *J. Am. Chem. Soc.*, 2007, **129**, 3315–3327.
37 K. Berlin, C. A. Castañeda, D. Schneidman-Duhovny, A. Sali, A. Nava-Tudela and D. Fushman, *J. Am. Chem. Soc.*, 2013, **135**, 16595–16609.
38 M.-Y. Lai, D. Zhang, N. LaRonde-LeBlanc and D. Fushman, *Biochim. Biophys. Acta BBA - Mol. Cell Res.*, 2012, **1823**, 2046–2056.
39 A. Hershko and A. Ciechanover, *Annu. Rev. Biochem.*, 1998, **67**, 425–479.
40 K. J. Walters, P. J. Lech, A. M. Goh, Q. Wang and P. M. Howley, *Proc. Natl. Acad. Sci. U. S. A.*, 2003, **100**, 12694–12699.
41 R. Varadan, M. Assfalg, A. Haririnia, S. Raasi, C. Pickart and D. Fushman, *J. Biol. Chem.*, 2004, **279**, 7055–7063.
42 D. Fushman, S. Cahill and D. Cowburn, *J. Mol. Biol.*, 1997, **266**, 173–194.
43 A. Abragam, *The principles of nuclear magnetism*, Clarendon Press ; Oxford University Press, Oxford [Oxfordshire]; New York, 1983.